



Characterization of precipitation and temperature equilibrium and its driving forces in the Yangtze river basin under climate change

Peng Yang^{1,2} · Yongyong Zhang³ · Jiang Li⁴ · Jun Xia¹ · Heqing Huang² · Yanchao Zhu²

Received: 22 May 2023 / Accepted: 6 July 2023 / Published online: 29 July 2023
© The Author(s), under exclusive licence to Springer-Verlag GmbH Germany, part of Springer Nature 2023

Abstract

Global warming has severely affected the climate in the Yangtze River Basin (YRB), resulting in complex and varying meteorological and hydrological processes. Therefore, identifying the effects of climate change in the YRB is important for characterizing the affected meteorological and hydrological processes. In this study, the characteristics of climate equilibrium were analyzed and the natural drivers of climate change in the YRB were explored using precipitation and temperature data from 1961 to 2018. The major findings can be summarized as follows. (1) Significant spatial and temporal differences in precipitation and temperature occurred. For example, annual precipitation showed a decreasing trend in the middle reaches but a significant increasing trend in the headwaters area and lower reaches. Between 1981 and 2001, annual precipitation and temperature exhibited overall increasing trends as well as abrupt changes. (2) Temporal changes in precipitation were primarily low in the middle and lower reaches and high in the headwater region of the YRB, although a low precipitation concentration degree (CD) occurred in summer in the upper reaches. High temperature changes over time mainly occurred in the headwater region of the YRB, although a high temperature CD occurred in winter in the northern parts. (3) Different teleconnection indices affected precipitation and temperature in different seasons. In particular, the Niño 3.4, North Atlantic Oscillation, and North Pacific Index had a significant influence on precipitation and temperature. This study provides critical information for revealing the changes in meteorological and hydrological processes and potential influencing factors in the YRB.

Keywords Climate change · Concentration degree · Spatial equilibrium · Yangtze River Basin

1 Introduction

Since before the industrial revolution, climate change has affected the climate system worldwide and impacted the atmosphere, ocean, and land, and its effects have increased along with the warming trend (IPCC 2018; CMA 2020). For example, thermodynamics can be used to explain the global increase in atmospheric water vapor, which has increased near the surface by approximately 7% per degree Celsius. Global precipitation and evaporation, which are constrained by the energy balance of the Earth, are increasing at a similar rate of 2–3% per degree Celsius under climate change (Allan et al. 2020). The decline in terrestrial water storage on the Qinghai–Tibet Plateau under the impact of climate change has been pronounced and will lead to a reduction in runoff to major rivers in the vicinity (e.g., Amu Darya and Indus basins), which will exacerbate the local water crisis (Li et al. 2023). The water shortage in the Halil River Basin in Iran is expected to increase with climate change-induced

✉ Peng Yang
yangpenghb@foxmail.com

✉ Yongyong Zhang
zhangyy003@igsnr.ac.cn

¹ State Key Laboratory of Water Resources and Hydropower Engineering Science, Wuhan University, Wuhan 430000, China

² Hubei Key Laboratory of Regional Ecology and Environmental Change, School of Geography and Information Engineering, China University of Geosciences, Wuhan 430074, China

³ Key Laboratory of Water Cycle and Related Land Surface Processes, Institute of Geographic Sciences and Natural Resources Research, Chinese Academy of Sciences, Beijing 100101, China

⁴ Information Center of Department of Natural Resources of Hubei Province, Wuhan 430071, China

impacts on precipitation, which represents a great threat to the sustainable development of this typically arid zone (Rafiei-Sardooi et al. 2022). Extreme precipitation and flooding events have intensified in all climate zones as water availability has increased in both wet and dry areas (Tabari et al. 2020).

Monsoon systems are a global earth climate pattern that couples the forced response of the climate system to the annual cycle of solar insolation (Wang et al. 2021a). Much of the Earth's surface, including areas and populations in South Asia, East Asia, Africa, Australia and North America, are affected by monsoon events (Wang et al. 2021a). However, monsoon regions are severely affected by climate change worldwide (Wang et al. 2021a). For example, a global downward trend in land-based monsoon precipitation has occurred, mainly because of a decline in the output of the Northern Hemisphere monsoon from the 1950 to 1980 s (Wang and Ding 2006). The Summer Monsoon circulation in South Asia has shown a clear downward trend since the 1950s, local meridional circulation has weakened, and precipitation has significantly decreased along the north-central and west coasts of India (e.g., Roxy et al. 2015), and these changes are attributable to the effects of anthropogenic aerosol forcing and equatorial Indian Ocean warming caused by increased abundance of greenhouse gases (e.g., Bollasina et al. 2011; Krishnan et al. 2016; Salzmann et al. 2014). The Summer Monsoon in East Asia has presented multi-decadal changes, with weakening circulation and a southern flooding and northern drought pattern occurring from the late 1970s to the end of the 20th century (Zhou et al. 2009; Ding et al. 2009). A re-greening has been observed in the Sahel region since the 1980s because of increases in total rainfall associated with positive trends in rainfall extremes (Panthou et al. 2014), strong mesoscale convective system frequency (Taylor et al. 2017), and average intensity (Lodoun et al. 2013; Taylor et al. 2017; Sarr et al. 2013). Over the past century, continued global warming and urbanization have led to significant increases in the characteristics of extreme rainfall events in monsoon regions, thus highlighting the importance of studying precipitation and temperature in the context of climate change.

The Yangtze River Basin (YRB) is situated in a subtropical zone in the low to mid-latitudes in China and represents a typical monsoon region of eastern China. It has been heavily influenced by climate change and experience significant anthropogenically influenced changes in precipitation and temperature (Yang et al. 2022a, c). For example, Jiang et al. (2008) demonstrated that the monthly precipitation concentration in the YRB varied significantly between 1961 and 2000, with the strongest relative increase detected in January and concentrated precipitation that causes seasonal flood hazards observed from April to August. Wang

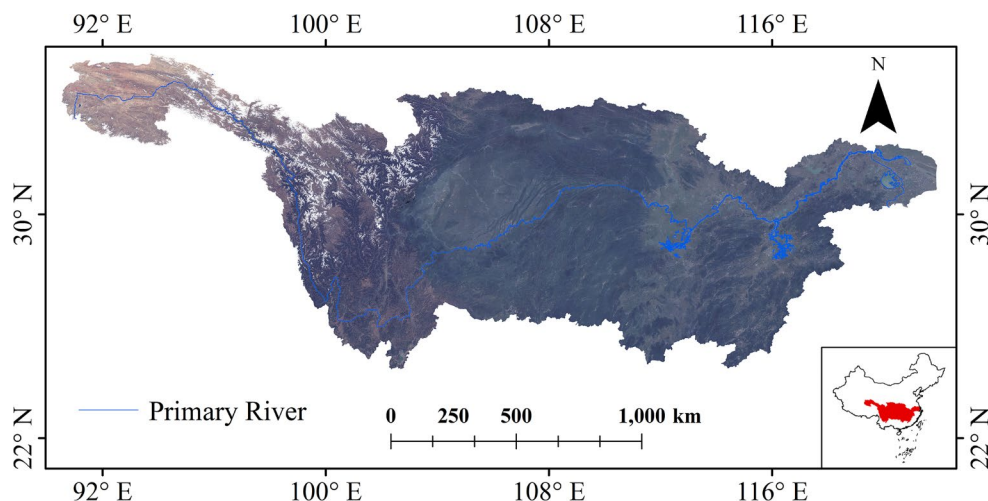
et al. (2021b) revealed that the reference evapotranspiration in the upper reaches of the YRB exhibited an increasing trend of 3.3 mm/year between 1951 and 2020. Yue et al. (2021) demonstrated that both precipitation and temperature changed significantly under different projected scenarios in the YRB. Considerable research has been conducted on the drivers of climate change in the YRB. For example, Yang et al. (2022a) found that teleconnection indices (e.g., Niño 3.4, Atlantic Multi-decadal Oscillation and North Pacific Index [NPI]) had a significant impact on drought-to-flood transitions in the YRB. Xiao et al. (2015) proposed that changes in precipitation in the YRB in different seasons can be attributed to different teleconnection indices (i.e., Indian Ocean Dipole, Pacific Decadal Oscillation [PDO], North Atlantic Oscillation [NAO], and El Niño/Southern Oscillation [ENSO]). Nie et al. (2020) demonstrated that climatic variability played a dominant role in the variability of outflows in most sub-basins. It should be noted that grey relational analysis provides a favorable method for analyzing the driving factors of climate change and surface processes (Yang et al. 2023). However, the focus in the YRB has been on precipitation, which is not distributed evenly in the region and is accompanied by abrupt changes in temperature. Additionally, previous studies have focused on the influence of only one teleconnection index on precipitation and temperature across the basin and neglected other teleconnection indices affecting different regions of the basin.

Therefore, this study addresses the following questions. (1) What are the characteristics of past climate change in the YRB? (2) How are the equilibrium features of precipitation and temperature manifested in the YRB? (3) What are the main drivers of climate change and how do they behave regionally in the YRB? This study is structured as follows. Section 2 provides an introduction to the regional characteristics of the YRB. Section 3 introduces the study data and methodology. Sections 4 and 5 present the findings and discussion, respectively. Section 6 provides the conclusions of the study.

2 Study area

The YRB is one of the most important economic and cultural regions in China (Fig. 1) (Zhang et al. 2022a; Wang et al. 2021b) and belongs to the subtropical monsoon climate zone, which has clear seasonal and regional characteristics defined by hot and humid summers and cold and dry winters (Yang et al. 2022c; Zhang et al. 2022b). The climate has a clear spatial distribution oriented in a north-south direction, with high temperatures and abundant precipitation in the south and low temperatures and relatively low precipitation in the north (Yang et al. 2022a; Liu et al. 2022). The

Fig. 1 The study area



temporal distribution of its climate types is characterized by relatively high temperatures and high water vapor content in the spring and summer months, which results in relatively high precipitation, particularly from June to August, which accounts for more than 60% of the annual precipitation. Low temperatures and low water vapor content distinguish the autumn and winter months, which experience low precipitation (Yang et al. 2022b; Jiang et al. 2008). However, the climate has also been influenced by significant global climate change in recent years, with increased precipitation in summer, an increase in the number of hot days, and less snowfall in winter (Zhao et al. 2022). In general, the YRB exhibits a variety of climatic characteristics, with the monsoon climate and distribution aspects serving as the most prominent features.

3 Materials and methods

3.1 Materials

3.1.1 Meteorological data

The meteorological data used in this study consisted of daily precipitation and temperature data from 1961 to 2018 downloaded from the China Meteorological Administration (<http://www.nmic.cn/data>), and they had a spatial resolution of 0.25°. This meteorological raster dataset in NetCDF format was converted with a high level of accuracy from actual measurements from 2,472 national weather stations, which have been used extensively in previous scientific studies (Yang et al. 2022c). Meteorological data were separated into annual (ANN) and seasonal scales for analysis, with spring, summer, autumn, and winter defined as March to May (MAM), June to August (JJA), September to November (SON), and December to February (DJF), respectively.

3.1.2 Teleconnection indices

Based on previous studies (e.g., Yang et al. 2022a; Xiao et al. 2015), we selected several teleconnection indices, namely the Niño 3.4, NPI, NAO, and PDO indices, as the alternative factors for driver analysis (<https://climatedataguide.ucar.edu/climate-data>). The seasonally and annually averaged values were then used as the seasonal and annual timescale teleconnection indices, respectively.

3.2 Methods

3.2.1 Temporal concentration degree of meteorological factors

To reveal the temporal equilibrium of climate change, this study was conducted using the information entropy index, namely the concentration degree (CD). In general, time series of climate factors are random, correlated, and abruptly variable between different moments (Galappaththi et al. 2019). Information entropy can demonstrate the occurrence of discrete random phenomena, with its value increasing as the uncertainty increases and vice versa (Sohoulande Djebou and Singh 2015). Information entropy can represent an effective expression of the CD of a time series and is calculated as follows (Li et al. 2017):

$$Q = 1 + \sum_{i=1}^N \frac{1}{\ln N} [C(x_i) \ln(x_i)] \quad (1)$$

, where i , N , x_i , $C(x_i)$, and Q are the element number, total number of elements, value of the i th element in the time series, contribution rate of x_i to the total amount, and CD over a certain period, respectively. The value of Q usually

ranges from 0 to 1, with lower values corresponding to a greater balance in the time series.

3.2.2 Spatial equilibrium degree (SED) of meteorological factors

SED is the proximity between any single element and the average of all elements in an overall space, and it is commonly used to detect the spatial equilibrium (Partridge et al. 2012; Zuo et al. 2019). Zuo et al. (2019) proposed a method of effectively specifying the spatial distribution of spatial factors, known as the SED method. The first step was to calculate the spatial equilibrium coefficient (SEC, A_{ij}) as follows:

$$A_{ij} = \begin{cases} 0, x_{ij} < \bar{x}_j - \Delta x_{ij1} \\ \frac{x_{ij} - \bar{x}_j + \Delta x_{ij1}}{\Delta x_{ij1}}, \bar{x}_j - \Delta x_{ij1} \leq x_{ij} \leq \bar{x}_j \\ \frac{\Delta x_{ij2} + \bar{x}_j - x_{ij}}{\Delta x_{ij2}}, \bar{x}_j \leq x_{ij} \leq \bar{x}_j + \Delta x_{ij2} \\ 0, x_{ij} > \bar{x}_j + \Delta x_{ij2} \end{cases} \quad (2)$$

,where x_{ij} , x_j , i , j , Δx_{ij1} , and Δx_{ij2} represent the data of the j th element of the i th station, average value of the j th factor over all stations, number of meteorological stations, number of climate elements, and increase or decrease compared with x_j , respectively. Owing to the large gap between the maximum and minimum values, we assume that $\Delta x_{ij1} = \Delta x_{ij2} = x_j$ (Li et al. 2021).

Subsequently, the SED can be calculated by Eq. (3):

$$B_j = \sum_{i=1}^N \frac{S_i}{S} A_{ij} \quad (3)$$

3.2.3 Cross-wavelet analysis

Both the degree of coherence between signals and the phase relationship between different time-series can be revealed via cross-wavelet analysis (Yang et al. 2022b), whereby the regions with large coefficients of variation indicate signals that are strongly correlated (Huang et al. 2015a, b, 2017). In this study, we analyzed the relationship between climate change and teleconnection indices and their periodic characteristics.

The spectral calculation between time series $x(t)$ and $y(t)$ can be obtained from Eq. (4) (Yang et al. 2022b):

$$W_{XY}(\alpha, \tau) = C_X(\alpha, \tau) C_Y^*(\alpha, \tau) \quad (4)$$

,where $C_Y^*(\alpha, \tau)$ represents the complex conjugate and $C_X(\alpha, \tau)$ represents the wavelet transform of $x(t)$.

The coherence, namely wavelet consistency (WTC, $R^2(\alpha, \tau)$), can be expressed as follows:

$$R^2(\alpha, \tau) = \frac{|S(a^{-1}W_{XY}(\alpha, \tau))|^2}{S(a^{-1}|W_X(\alpha, \tau)|^2) S(a^{-1}|W_Y(\alpha, \tau)|^2)} \quad (5)$$

,where S denotes the smooth operator.

3.2.4 Grey relational analysis

To analyze the degree of correlation between teleconnection indices and climate change in the YRB based on raster data, this study explored the drivers in regional areas across the basin based on grey relational analysis, which can quantitatively describe the relative changes and associated factors (Yang et al. 2023). Strong correlations indicate a largely similar pattern of change with a high degree of variation (Yang et al. 2023). The specific principles are as follows.

Assume that the system time series is X_0 , where $X_0 = (x_0(t))$. For a given sequence of correlation factors X_i , there are various time delays. For a given sequence of correlation factors X_i with different time delays, a sequence of correlated factor behaviors with time delays $X_{i\tau} = (x_i(t-\tau))$, where $\tau = 0, 1, 2, \dots, k$, is obtained, with X_i and $X_{i\tau}$ constituting the study set. The grey relational analysis method can be expressed in the following computational steps:

$$X_0 = (x_0(t)), t = 1, 2, \dots, n \quad (6)$$

$$X_{i\tau} = (x_i(t-\tau)), \tau = 1, 2, \dots, k \quad (7)$$

where τ is the lag time of $X_{i\tau}$ relative to X_0 .

First, we preprocessed X_0 and $X_{i\tau}$ to determine the average:

$$X'_0 = (x'_0(t)) = \frac{X_0}{n}, t = 1, 2, \dots, n \quad (8)$$

$$X'_{i\tau} = (x'_{i\tau}(t-\tau)) = \frac{X_{i\tau}}{x_{i\tau}}, t = 1, 2, \dots, n; \tau = 1, 2, \dots, k \quad (9)$$

where \bar{x}_0 is the mean of sequence X_0 , and $\bar{x}_{i\tau}$ represents the mean of sequence $X_{i\tau}$.

The correlation between X_0 and $X_{i\tau}$ at t can be expressed as follows:

$$\gamma(x'_0(t), x'_{i\tau}(t-\tau)) = \frac{\min_t \max_t |x'_0(t) - x'_{i\tau}(t-\tau)| + \max_t \max_t |x'_0(t) - x'_{i\tau}(t-\tau)|}{|x'_0(t) - x'_{i\tau}(t-\tau)| + \max_t \max_t |x'_0(t) - x'_{i\tau}(t-\tau)|} \quad (10)$$

.The grey relational correlation between $X_{i\tau}$ and X_0 can be obtained using Eq. (11):

$$\gamma(X_0, X_{i\tau}) = \frac{1}{n} \sum_{t=1}^n \gamma(x'_0(t), x'_{i\tau}(t-\tau)), \tau = 1, 2, \dots, k \quad (11)$$

where γ and $\gamma(X_0, X_{i\tau})$ denote the grey correlation and maximum correlation at the corresponding time lag periods of X_0 and X_i , respectively.

4 Results

4.1 Temporal and spatial variations in temperature and precipitation in the YRB

Figure 2 displays the variations in precipitation in the YRB from 1961 to 2018. The maximum precipitation in ANN in the lower reaches of the YRB exceeded 2,000 mm, which was significantly higher than that in the central and western regions, whereas the minimum was close to 0 (Fig. 2a). In addition, a clear upward trend was observed in the western part, with a maximum trend of 8 mm/a, and a clear downward trend was observed in the middle parts, with a maximum trend of -4 mm/a (Fig. 2b). Precipitation in ANN showed an overall upward trend from 1968 to 2018, with significant abrupt changes ($p < 0.05$) around 1985 and 2001 (Fig. 2c). MAM precipitation was similar to that of ANN; for example, more precipitation was observed in the east (i.e., maximum of approximately 600 mm) while less was observed in the west (i.e., minimum of approximately 0 mm), and a significant increase of up to 2 mm/a was observed in the west while a significant decrease of up to -2 mm/a was observed in the central region (Fig. 2d and e). Additionally, a significant and abrupt change was observed in 2015 (Fig. 2f). In contrast, the precipitation in JJA was significantly higher throughout the YRB, with slightly lower values observed in the source areas, significantly higher values observed in the eastern regions (maximum near 800 mm), and scattered

values observed in the western regions, where precipitation decreased significantly ($p < 0.05$) (Fig. 2g h). As for the time series, abrupt changes occurred between 1981 and 1991 and an upward trend occurred from 1961 to 2018 (Fig. 2i). The spatial distribution of precipitation was less varied during SON, with several scattered areas of significantly reduced precipitation in the south-central region and significantly increased precipitation in the sub-regions of the headwaters area (Fig. 2j and k). Regarding the time-series variability, precipitation during SON varied little and did not show abrupt changes from 1961 to 2018 (Fig. 2l). However, precipitation in DJF presented large spatial regional differences, with significantly more precipitation in the east than that in the south-central and west regions and a scattered distribution of significantly less precipitation in the center, with several abrupt changes occurring before 1991 (Fig. 2m and o).

Figure 3 shows the spatial and temporal characteristics of temperature in the YRB from 1961 to 2018. The study found that the ANN and seasonal temperatures in the YRB were higher in the central-eastern region than those in the western headwaters, with the lowest temperatures occurring in the headwaters in winter and reaching -15 °C and the highest temperatures occurring in the eastern region in summer and reaching 25 °C (Fig. 3a and d g, 3j, and 3m). Regarding spatial changes, the ANN, MAM, SON, and DJF temperatures displayed significant increasing trends ($p < 0.05$) throughout the YRB, with a maximum increase

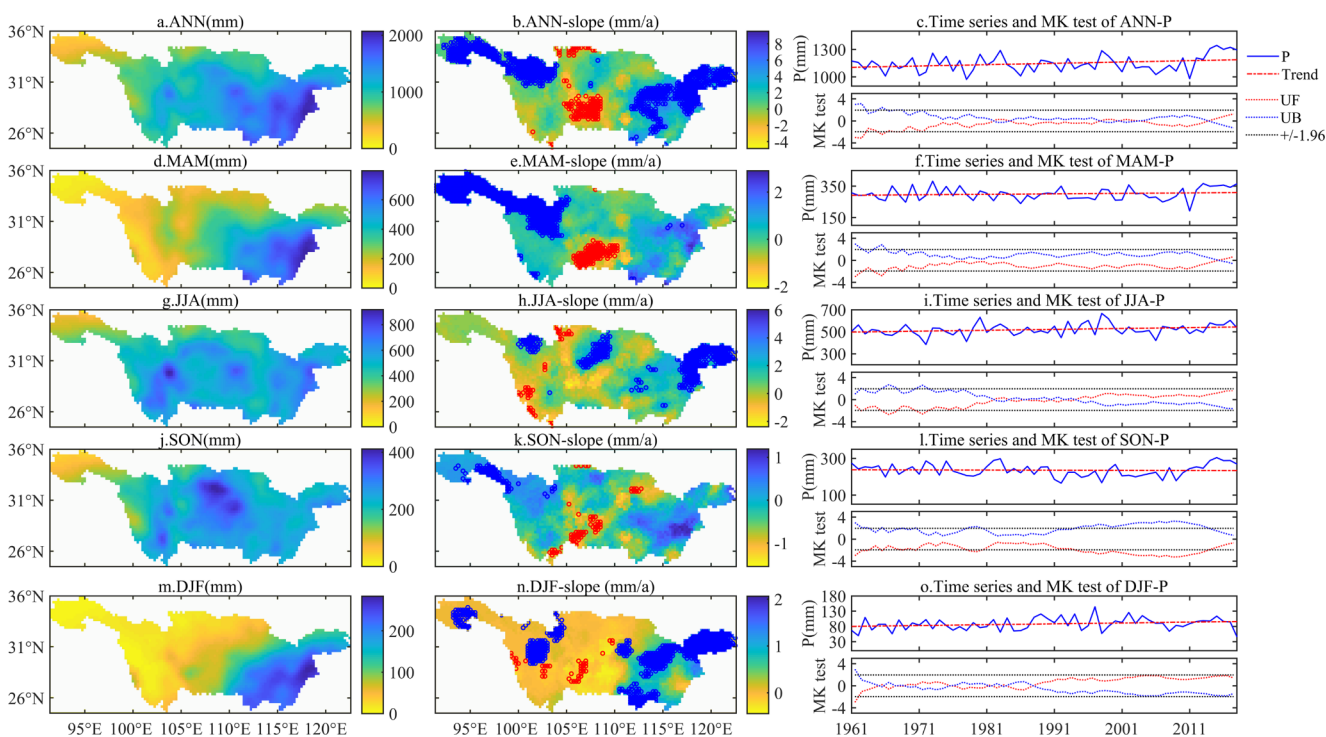


Fig. 2 Temporal and spatial variability of precipitation in the YRB during 1961–2018

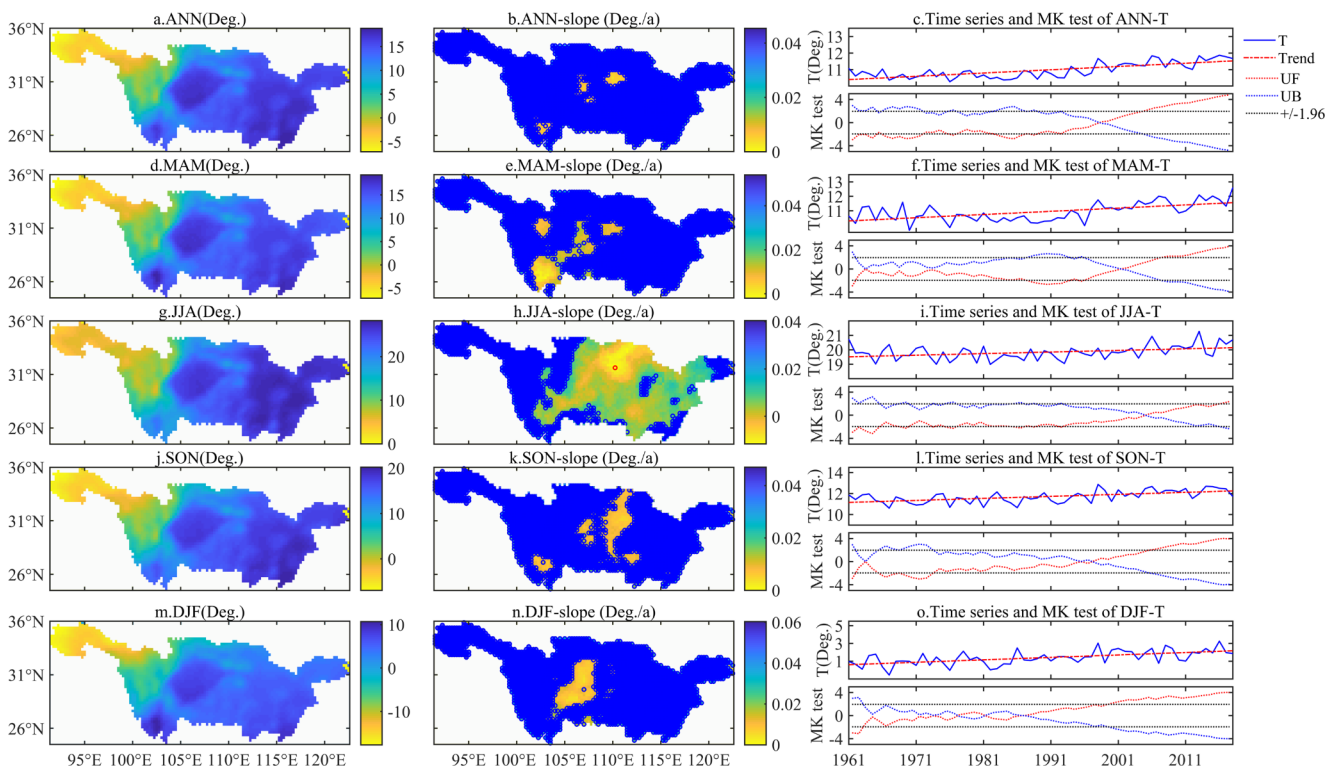


Fig. 3 Temporal and spatial variability of temperature in the YRB during 1961–2018

of $0.06\text{ }^{\circ}\text{C/a}$. In JJA, precipitation only exhibited an obvious upward trend in the headwaters of the YRB ($p < 0.05$), whereas that in the other regions presented insignificant change (Fig. 3b and e, h, 3k, and 3n). For the temperature time series, a significantly upward trend and abrupt changes were observed for the ANN, MAM, JJA, SON, and DJF periods in 1998, 2001, 2005, 1995, and 1985, respectively.

4.2 Precipitation and temperature equilibrium in the YRB under climate change

Figure 4 shows the spatial CD of temperature and precipitation in the YRB. The CD of ANN, MAM, SON, and DJF precipitation was small in the east, with a minimum close to 0, and large in the northwest, with a maximum close to 0.4. This indicates that ANN and MAM precipitation in the eastern region of the YRB was more uniform than that in the west. The opposite was true in JJA, with the CD of precipitation being large in the east, with a maximum of 0.15, and small in the west, with values close to 0. For the CD of temperature in the YRB, larger ANN, MAM, JJA, SON, and DJF values were located in the eastern regions, with a maximum of 0.3, while smaller values were mainly located

in the eastern regions, with a minimum close to 0. This indicates that the temperature changes were more uniform in the lower reaches. Regarding the time series of CD, significant fluctuations in precipitation and temperature were observed for ANN and seasons, with negative correlations observed from 1961 to 1981 and 2001 to 2018 for the CD of ANN, MAM, and SON values and positive correlations observed from 1981 to 2001 (Fig. 4c and f, and 4L). Precipitation and temperature in JJA and DJF were positively correlated with each other from 1961 to 2018 (Fig. 4i and o).

Figure 5 shows the SEC and SED of precipitation and temperature in the YRB from 1968 to 2018. The study found that the SEC of ANN, MAM, and DJF precipitation was small in the headwaters and downstream, indicating significant spatial variability in precipitation in the region, whereas the SEC of precipitation was obvious high in the middle reaches (Fig. 5a and d, and 5m). However, the SEC of precipitation in JJA and SON was small, demonstrating that precipitation in these periods was spatially consistent, with both representing rainy seasons (Fig. 5g and j). Regarding the SEC of temperature, large ANN, MAM, JJA, and SON values were concentrated in the Sichuan Basin and its surrounding areas, with a maximum of approximately

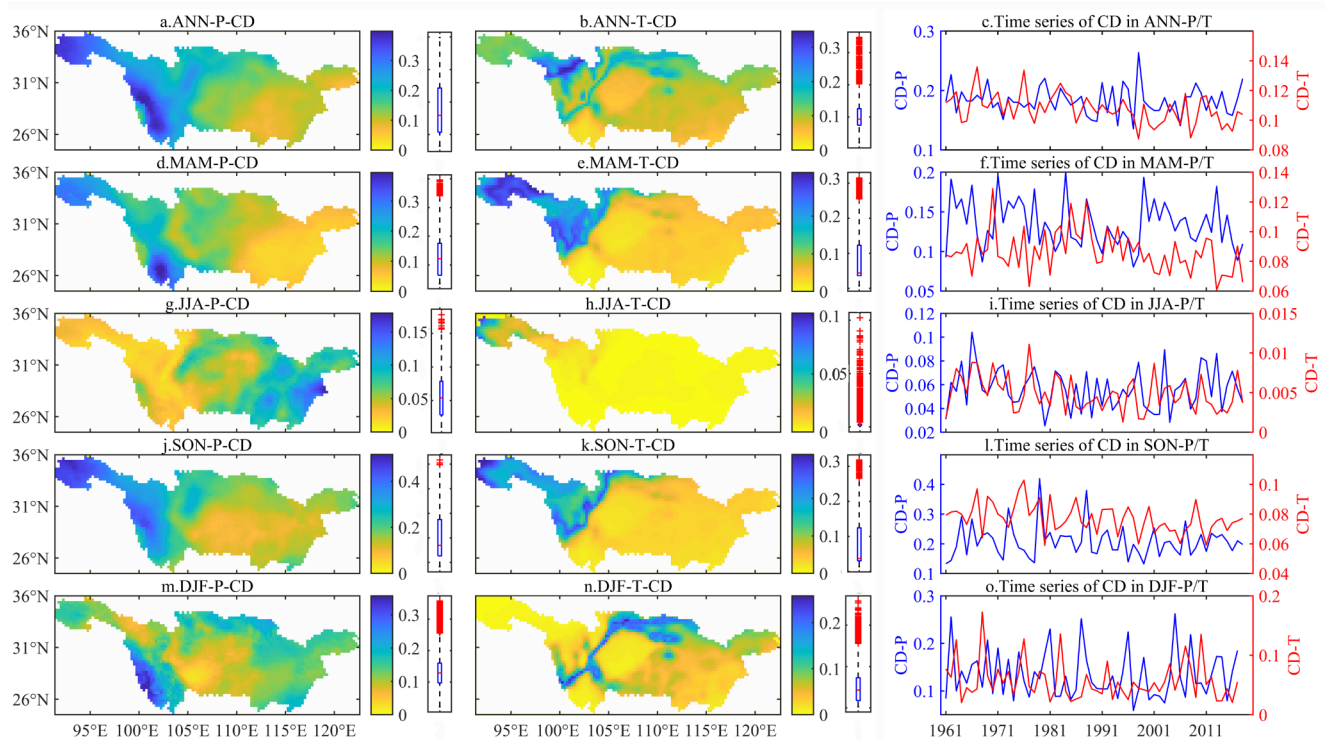


Fig. 4 Spatial and temporal characteristics of the concentration degree of precipitation and temperature in the YRB during 1961–2018

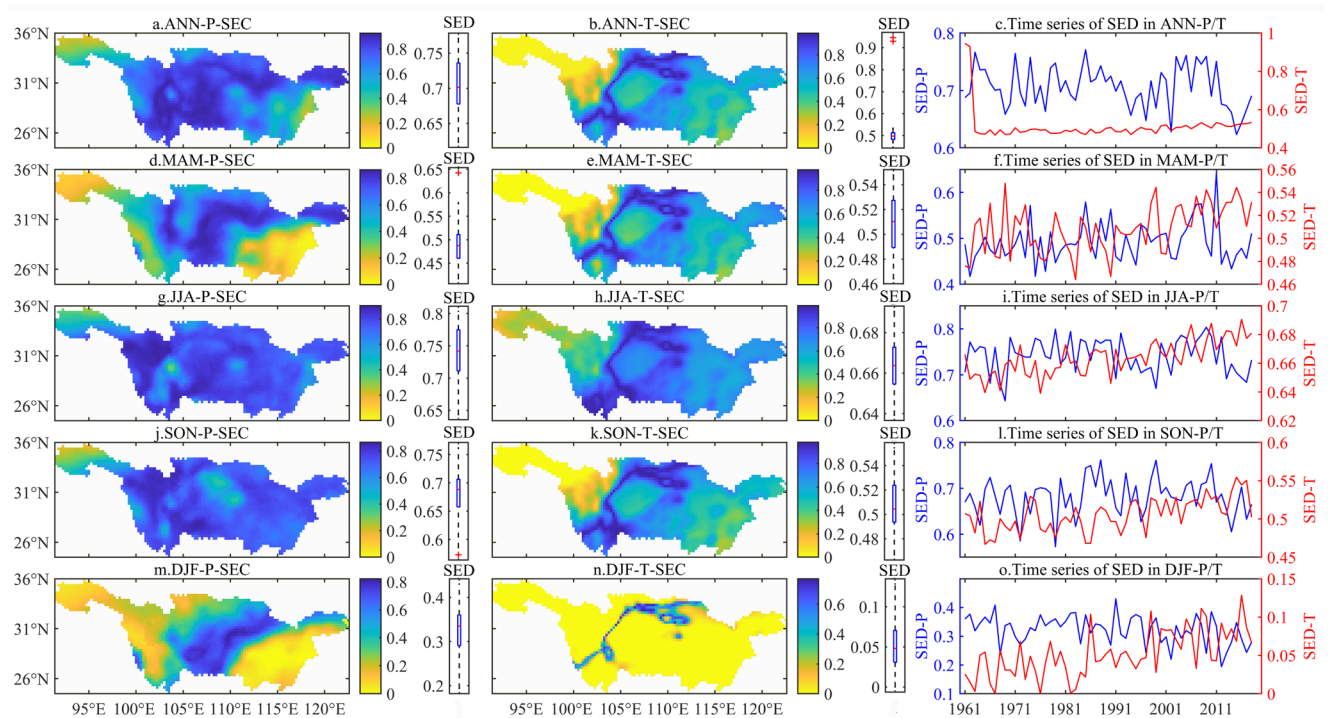


Fig. 5 Spatial and temporal characteristics of the SED of precipitation and temperature in the YRB during 1961–2018

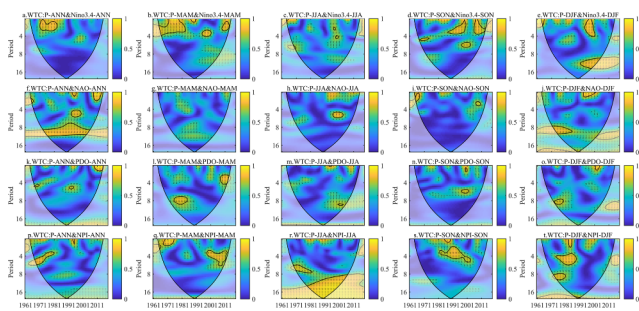


Fig. 6 Wavelet coherence (WTC) analysis of precipitation with teleconnection indices in the YRB during 1961–2018

0.8, while small values were concentrated in the headwaters, with a minimum of approximately 0 (Fig. 5b and e, h, and 5k). For temperature in DJF, large SEC values were mainly concentrated in the northern part of the YRB, indicating that the SED of ANN, MAM, JJA, and SON temperature was balanced in the middle and lower reaches and presented small differences regionally but large differences in the headwaters. For the ANN time series of the SED, the SED of temperature varied significantly less than that of precipitation. The SED of precipitation and temperature in MAM, JJA, and DJF exhibited a significantly negative correlation between 1961 and 2018, whereas that in SON displayed a negative correlation between 1961 and 1985 and positive correlation between 1981 and 2018. These findings illustrate the significant spatial variation in precipitation and temperature occurred in the YRB across seasons and years.

4.3 Response of climate change to teleconnection indices in the YRB

Figure 6 presents the WTC for the precipitation and teleconnection indices (e.g., PDO, NAO, Niño 3.4, and NPI) in the YRB from 1968 to 2018. The ANN precipitation was significantly correlated with the Niño 3.4 on a 1–2-year scale from 1971 to 1981, with the NAO on a 10-year time period from 1971 to 2011 (coefficient > 0.8), and with the NPI on a 2–6-year scale from 1971 to 1981. Precipitation in MAM was obviously correlated with the Niño 3.4 on a 1–4-year scale between 1961 and 1985 and consistent with the PDO on a 6–9-year scale between 1975 and 1985 and 2–5-year scale between 2001 and 2011. Precipitation in JJA was consistent with the NAO on a 5–6-year scale between 1991 and 2001 and significantly correlated with the NPI on a 5–7-year scale from 1965 to 1981 and 8–16-year scale from 1981 to 2005. Precipitation in SON was significantly correlated with the Niño 3.4 on a 2–4-year scale from 1981 to 2005 (correlation coefficient of 0.8 or greater) and with the NPI on a 3–5-year scale from 1981 to 2001. Precipitation in DJF was significantly correlated with the four teleconnection indices PDO, Niño 3.4, NAO, and the NPI on a 2–4-year scale from

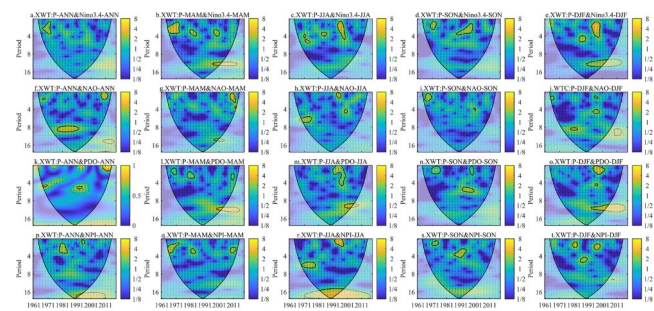


Fig. 7 Cross wavelet transform (XWT) analysis of precipitation with teleconnection indices in the YRB during 1961–2018

1995 to 2001, 10–16-year scale from 1991 to 2001, 8–10-year scale from 1971 to 1985, 8–10-year scale from 1981 to 1985, and 1–2-, 4–6-, 8–9-, and 10-year scale from 1971 to 1985, with correlation coefficients > 0.8.

Figure 7 shows the cross-wavelet analysis of the precipitation and teleconnection indices during 1968–2018. ANN precipitation showed a significantly negatively correlation with the Niño 3.4 on a 2–4-year scale from 1971 to 1981, a significantly positive correlation with the NAO on a 6–8-year scale from 1975 to 1995, and a negative correlation with the NPI on a 2–4-year scale from 1978 to 1985. The precipitation in MAM showed a significantly negative correlation with the Niño 3.4 on a 2–4-year scale from 1965 to 1975 and with the PDO on a 3–4-year scale from 1978 to 1985; however, it exhibited a significantly positive correlation with the NPI on a 2–3-year scale from 1965 to 1975. Precipitation in JJA showed a significantly negative correlation with the Niño 3.4 on a 2–4-year scale from 1991 to 2001, with the NAO on a 5–7-year scale between 1971 and 1981, and with the PDO on a 1–5-year scale between 1991 and 2001, and it exhibited a significantly positive correlation with the NPI on a 1–3-year scale between 1985 and 1995 and 5–7-year scale between 1971 and 1981. Precipitation in SON was significantly positively correlated with the Niño 3.4 on a 2–5-year scale between 1981 and 2001, with the NAO on a 1–2-year scale between 1965 and 1971, with the PDO on a 1–2-year scale between 1971 and 1975 and 5–6-year scale between 1985 and 1995, and with the NPI on a 3–5-year scale between 1985 and 1995. Precipitation in DJF was positively correlated with the Niño 3.4 on a 2–4-year scale between 1991 and 1995 and on a 10–14-year scale between 1985 and 2001, with the PDO on a 1–3-year scale between 1991 and 1995 and 9–12-year scale between 1991 and 2001, and consistent with the NPI on a 2–3-year scale between 1981 and 1985 and 4–6-year scale between 1985 and 1991.

Figure 8 shows the WTC analysis of the temperature and teleconnection indices. Temperature in ANN was significantly positively correlated with the Niño 3.4 on a 1–8-year scale between 1961 and 1971 and 3–4-year scale between

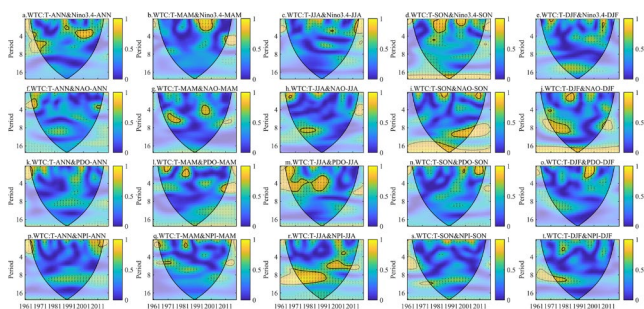


Fig. 8 Wavelet coherence (WTC) analysis of temperature with teleconnection indices in the YRB during 1961–2018

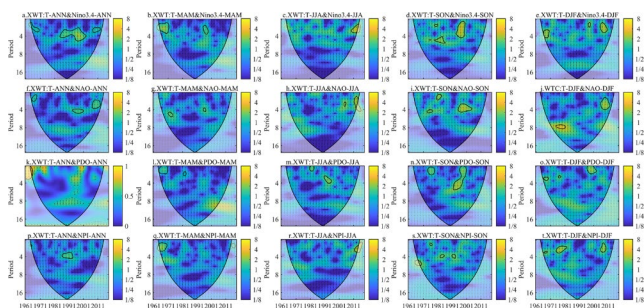


Fig. 9 Cross wavelet transform (XWT) analysis of temperature with teleconnection indices in the YRB during 1961–2018

1995 and 2005 (coefficient of approximately 0.8), significantly positively correlated with the NAO on a 3–4-year scale between 1968 and 1975, and significantly related to the NPI on a 1–2-year scale between 2007 and 2011. Temperature in MAM was significantly positively correlated with the Niño 3.4 on a 1–4-year scale between 1991 and 2001, with the NAO on a 5–7-year scale between 1971 and 1981 and 3–6-year scale between 1995 and 2001, and was significantly related to the PDO on a 1–2-year scale between 1968 and 1973 and 2–3-year scale between 1981 and 1985. Temperature in JJA was significantly correlated with the NAO on a 8–10-year scale between 1975 and 1985, with the PDO on a 1–6-year scale between 1961 and 1985 and 3–6-year scale between 1981 and 1991, and with the NPI on a 6–10-year scale between 1961 and 1991, and 5–7-year scale between 1991 and 2011. Temperature in SON was significantly correlated with the Niño 3.4 on a 1–3-year scale between 1981 and 1991 and 1–2-year scale between 1995 and 2001, with the NAO on 1–2-year scale between 1988 and 1991 and 6–8-year scale between 1991 and 2018, and with the PDO on a 1–3-year scale between 2005 and 2015. Temperature in DJF was significantly correlated with the Niño 3.4 on a 1-year scale between 1969 and 1972, with the NAO on a 6–9-year scale between 1965 and 1985 and 1–2-year scale between 1981 and 1985, with the PDO on a 1–3-year scale between 1995 and 2001, and with the NPI on a 8–10-year scale between 1971 and 1985.

Figure 9 shows the cross-wavelet transform (XWT) of the temperature and teleconnection indices for the YRB during 1968–2018. Temperature in ANN was consistent with the Niño 3.4 on a 3–6-year cycle during 1985–2005, with the NAO on a 4–5-year cycle during 1992–1997 and 3–5-year cycle during 2005–2011, and with the NPI on a 3–5-year cycle during 1985–1995. Temperature in MAM was consistent with the Niño 3.4 on a 2–4-year cycle during 1965–1971 and 3–4-year cycle during 1995–1999, and with the PDO and NPI on a 2–4-year cycle during 1965–1970. Temperature in JJA was consistent with the Niño 3.4 and NAO on a 2–3-year cycle during 2008–2011 and with the PDO on a 2–3-year cycle during 1985–1993. Temperature in SON was correlated with the Niño 3.4 on a 2–5-year cycle during 1992–2001, with the NAO on a 2–4-year cycle during 1995–2005, and with the PDO on a 1–3 year time cycle during 1972–1976 and 1–6-year cycle during 1992–2005. Temperature in DJF was connected with the Niño 3.4 on a 3–4-year cycle during 1971–1975 and on a 2–3 cycle during 2005–2008, with the NAO over a 7–9-year cycle during 1975–1981 and 2–4-year cycle during 2005–2011, with the PDO over a 1–3-year cycle during 1995–2001, and with the NPI over a 2–4-year cycle during 1975–1985 and 2–4-year cycle during 2005–2008.

Figure 10 depicts the grey relation analysis between precipitation/temperature and teleconnection indices during 1968–2018. For the ANN temperature in the YRB, almost the entire basin was influenced by the NAO, while the other teleconnection indices did not demonstrate much influence (Fig. 10a). For precipitation in MAM, the middle and lower reaches were mainly influenced by the Niño 3.4, whereas the middle and upper reaches were mainly influenced by the NPI. The alternative PDO did not have much influence on precipitation in MAM (Fig. 10c). Regarding precipitation in JJA, SON, and DJF, respectively, the entire YRB was mainly influenced by the NPI, Niño 3.4, and NPI, respectively. Regarding the ANN temperature, the entire basin was mainly influenced by the NAO, whereas the other alternative teleconnection indices were insignificant (Fig. 10b). For temperature in MAM, the vast majority of the YRB was influenced by the Niño 3.4 while only a small section in the headwater region was affected by the NPI (Fig. 10f). For temperature in SON, the YRB was mainly influenced by the PDO, with a few scattered grids in the headwaters showing the influence of the Niño 3.4. Precipitation in DJF in the YRB was mainly influenced by the NPI, with only a few scattered grids being influenced by the Niño 3.4 (Fig. 10h and j). In summary, precipitation and temperature in the YRB were influenced by different teleconnection indices during different seasons.

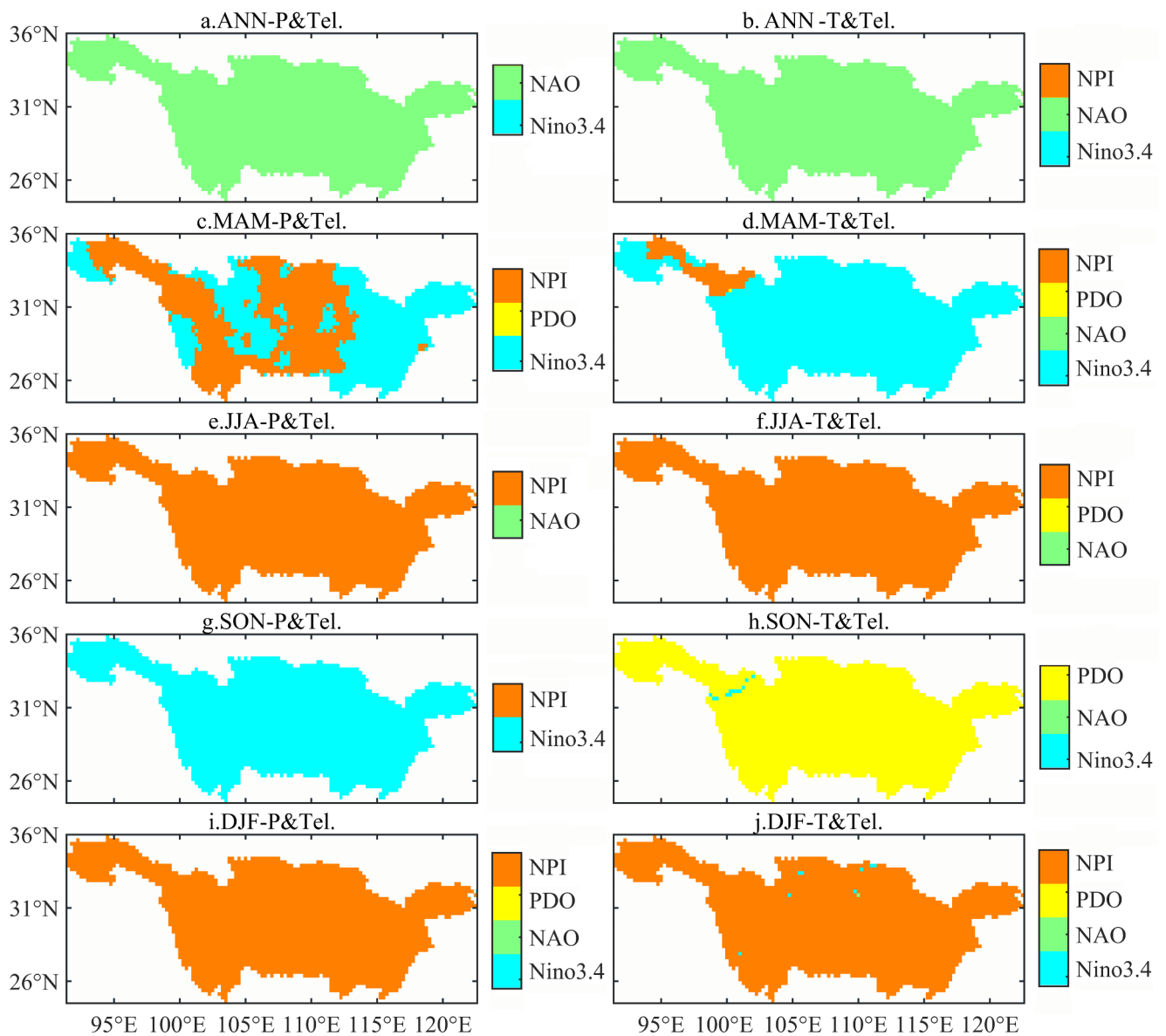


Fig. 10 Grey relation analysis of precipitation and temperature with remote correlation indices in the YRB at grid scale

5 Discussion

5.1 The evidence about climate change in the YRB

The climate of the YRB has changed considerably since the past (Yang et al. 2022a, b). In the time series, ANN and seasonal precipitation in the YRB showed an upward trend from 1961 to 2018 and across the basin. Similarly Yang et al. (2022a, b) observed a clear trend of increasing precipitation and temperature in the YRB under changing environmental conditions. Furthermore, Hu et al. (2021) found a downward trend in trace precipitation and an upward trend in extremely heavy precipitation in the YRB, which is consistent with the results of Chen et al. (2020), thus revealing a

gradual increase in extreme precipitation from the middle to the lower reaches. A significant upward trend in temperature was observed, which was also demonstrated by Niu et al. (2020), who observed an increasing rate of approximately 0.15–0.38 °C/decade. All temperature extremes in the YRB changed considerably (Niu et al. 2020; Shi et al. 2021a), with an extremely significant trend of increasing temperatures. The dry–wet alternation in the YRB also showed significant changes under climate change (Yang et al. 2022a), which correlated with an increased occurrence of natural disasters, such as floods and droughts (Jiang et al. 2008; Yang et al. 2022a), and altered temperatures of water bodies and ecological characteristics of vegetation in the YRB (Yang et al. 2011; Tao et al. 2020; Shi et al. 2021b; Gemmer

et al. 2008; Zhang et al. 2019). Studies have also suggested that precipitation and temperature in the YRB will be more complex under continued climate change (Tao et al. 2012). Therefore, it is necessary to address climate change in the YRB.

5.2 Precipitation and temperature equilibrium in the YRB

CD and SED are typically introduced to explore the equilibrium properties of climate change, and they indicate that climate change mainly depends on the degree of spatial and temporal equilibrium of both precipitation and temperature (Martin-Vide 2004; Zhang et al. 2003). CD mainly reflects the temporal concentrations of precipitation and temperature, whereas SED mainly denotes the spatial concentrations of precipitation and temperature (Zuo et al. 2019; Wu et al. 2022). Although differences have been observed, Liu et al. (2022) observed a CD threshold ranging from 0.1 to 0.3 and SED values ranging from 0.4 to 0.7, which is consistent with the results of this study. Although limited research has been performed on the spatiotemporal balance of precipitation and temperature in the YRB, changes in other indicators effectively reflect the spatiotemporal characteristics of climate change. For example, Yang et al. (2022a) revealed similarities between the dry-wet changes and the features of precipitation and temperature change. Furthermore, Yang et al. (2022c) demonstrated that the spatial and temporal characteristics of the flood potential index and soil moisture in the YRB were similar to those of the precipitation and temperature equilibrium. Notably, precipitation and temperature do not always vary positively or negatively in the YRB, particularly because the interrelationship between precipitation and temperature in some specific seasonal time series is not always consistent over a given period. For a typical monsoon basin, the CD/SED values and their variability in terms of precipitation and temperature represent the spatial and temporal distribution and variability of water resources in the basin (Zuo et al. 2019). Therefore, exploring the changes in the CD and SED values of precipitation and temperature in the basin is important for managing and planning water resources.

5.3 Impacts of teleconnection indices on climate change in the YRB

In this study, precipitation and temperature in the YRB were influenced by a variety of teleconnection indices, which affected precipitation and temperature in different regions and seasons. For example, ANN precipitation and temperature changes were influenced by the NAO, whereas precipitation and temperature in other seasons were influenced by

the NPI and Niño 3.4. This result was confirmed by Xiao et al. (2015), who found that the dominant factor for seasonal precipitation was the ENSO, which was also influenced by the PDO and NAO. Moreover, Ouyang et al. (2014), Peng et al. (2018), and Wei et al. (2020) found that the ENSO and PDO not only affected changes in precipitation but also changes in runoff in the YRB, especially in non-ENSO years, when the PDO played a significant role (Dong 2016). Tang et al. (2021) revealed that the temperature in the middle reaches of the YRB was also influenced by the ENSO through the western Pacific circulation. Shi and Cui (2022) argued that El Niño had a more pronounced effect on precipitation than that on temperature and had a greater effect on seasonal temperatures and precipitation in the YRB than La Niña, which is consistent with our findings. Furthermore, Blender et al. (2011) demonstrated the long history of the impact of the ENSO on precipitation, temperature, and runoff in the YRB. Moreover, dry-wet variations in the YRB are also evident based on the teleconnection indices (Yang et al. 2022a). Overall, teleconnection indices had a significant impact on climate change in the YRB, and studies on climate change in this region need to focus on teleconnection index changes and oceanic oscillations.

6 Conclusion

Climate change has important implications for eco-hydrological processes in the YRB. We detected the characteristics of climate equilibrium and explored the natural drivers of climate change based on the features of precipitation and temperature in the basin from 1961 to 2018. The major findings are as follows.

(1) Significant spatial and temporal differences in precipitation and temperature occurred in the YRB. ANN precipitation showed a decreasing trend, mainly in the middle reaches, a significantly increasing trend in the headwater area and lower reaches, and an overall increasing trend with abrupt changes between 1981 and 2001. The entire YRB displayed an increasing trend for ANN temperature, with abrupt changes between 1991 and 2001.

(2) With the exception of the CD of precipitation in JJA, which was low in the upper reaches of the YRB, precipitation was low in the middle and lower reaches and high in the upper reaches during other temporal periods. The high concentration of temperature was mainly focused in the upper reaches of the YRB, except for the CD of temperature in DJF, which was distributed in the northern parts of the YRB. In terms of time series, the CD of precipitation and temperature in MAM showed a negative correlation from 1996 to 2018 but fluctuated consistently in terms of both precipitation and temperature over the other time series.

(3) Precipitation and temperature in the YRB were influenced by different teleconnection indices in different seasons. In particular, the Niño 3.4, NPI, and NAO had significant effects on precipitation and temperature in the YRB. Grey rational analysis indicated that the NAO showed significant correlations with ANN precipitation and temperature over the entire YRB, whereas the NPI was significantly associated with MAM precipitation and temperature in the middle and upper reaches and with JJA and DJF precipitation and temperature over the basin. The Niño 3.4 index was significantly associated with MAM precipitation and temperature in the middle and lower reaches of the YRB.

Author contributions All authors contributed to the study conception and design. Material preparation, data collection and analysis were performed by JL and YCZ. The first draft of the manuscript was written by PY and YYZ. JX and HQH performed as the program administration and all authors commented and on previous versions of the manuscript.

Funding This research was supported by the Visiting Researcher Fund Program of the State Key Laboratory of Water Resources and Hydro-power Engineering Science (2020SWG01).

Data availability Meteorological data are supported by China Meteorological Administration (available at <http://data.cma.cn>). Teleconnection indices are provided by the National Center for Atmospheric Research (available at <https://climatedataguide.ucar.edu/climate-data>).

Declarations

Conflict of interest The authors declare no competing interests.

References

- Allan RP, Barlow M, Byrne MP et al (2020) Advances in understanding large-scale responses of the water cycle to climate change. *Anal New York Acad Sci* 1472(1):49–75
- Blender R, Zhu XH, Zhang D et al (2011) Yangtze runoff, precipitation, and the east asian monsoon in a 2800 years climate control simulation. *Quatern Int* 244(2):194–201
- Bollasina MA, Ming Y, Ramaswamy V (2011) Anthropogenic aerosols and the weakening of the south asian summer monsoon. *Sci* 334:502–505. <https://doi.org/10.1126/science.1204994>
- Chen ZQ, Zeng Y, Shen GY et al (2020) Spatiotemporal characteristics and estimates of extreme precipitation in the Yangtze River Basin using GLDAS data. *Int J Climatol* 41:E1812–E1830
- CMA Climate Change Center (20202020) *Blue Book on Climate Change in China*. Science Press, Beijing
- Ding Y, Sun Y, Wang Z et al (2009) Inter-decadal variation of the summer precipitation in China and its association with decreasing asian summer monsoon part II: possible causes. *Int J Climatol* 29:1926–1944. <https://doi.org/10.1002/joc.1759>
- Dong X (2016) Influences of the Pacific Decadal Oscillation on the east asian summer monsoon in non-ENSO years. *Atmos Sci Lett* 17(1):115–120
- Galappaththi EK, Ford JD, Bennett EM (2019) A framework for assessing community adaptation to climate change in a fisheries context. *Environ Sci Pol* 92:17–26. <https://doi.org/10.1016/j.envsci.2018.11.005>
- Gemmer M, Tong J, Su B et al (2008) Seasonal precipitation changes in the wet season and their influence on flood/drought hazards in the Yangtze River Basin, China. *Quatern Int* 186(1):12–21
- Hu M, Dong M, Tian X et al (2021) Trends in different grades of precipitation over the Yangtze River Basin from 1960 to 2017. *Atmos* 12(3):413
- Huang SZ, Chang JX, Huang Q et al (2015a) Identification of abrupt changes of the relationship between rainfall and runoff in the Wei River basin, China. *Theor Appl Climatol* 120(1–2):299–310
- Huang SZ, Chang JX, Leng GY et al (2015b) Integrated index for drought assessment based on variable fuzzy set theory: a case study in the Yellow River basin, China. *J Hydrol* 527:608–618
- Huang SZ, Li P, Huang Q et al (2017) The propagation from meteorological to hydrological drought and its potential influence factors. *J Hydrol* 547:184–195
- IPCC. Summary for policymakers (2018) In: Masson-Delmotte V, Zhai P, Pörtner H-O et al (eds) *Global warming of 1.5°C*. Cambridge University Press, Cambridge and New York, pp 1–24
- Jiang T, Kundzewicz ZW, Su B (2008) Changes in monthly precipitation and flood hazard in the Yangtze River Basin, China. *Int J Climatol* 28
- Krishnan R, Coauthors (2016) Deciphering the desiccation trend of the south asian monsoon hydroclimate in a warming world. *Clim Dyn* 47:1007–1027
- Li H, Zhai PM, Zhao W et al (2017) Changes in temporal concentration property of summer precipitation in China during 1961–2010 based on a new index. *J Meteorol Res* 31:336–349
- Li QW, Zuo QT, Li DL et al (2021) Spatial equilibrium analysis of water resources development and utilization in Xinjiang. *Water Res Protect* 37:28–33
- Li XY, Long D, Scanlon BR et al (2023) Climate change threatens terrestrial water storage over the Tibetan Plateau. *Nat Clim Change* 12(9):801–. <https://doi.org/10.1038/s41558-022-01443-0>
- Liu YJ, Yang P, Zhang SQ et al (2022) Dynamic identification and health assessment of wetlands in the middle reaches of the Yangtze River under changing environment. *J Clean Prod*. <https://doi.org/10.1016/j.jclepro.2022.131105>
- Lodoun T, Giannini A, Traorei PS et al (2013) Changes in seasonal descriptors of precipitation in Burkina Faso associated with late 20th century drought and recovery in West Africa. *Environ Dev* 5:96–108
- Martin-Vide J (2004) Spatial distribution of a daily precipitation concentration index in peninsular Spain. *Int J Climatol* 24:959–971
- Nie N, Zhang WC, Liu M et al (2020) Separating the impacts of climate variability, land-use change and large reservoir operations on streamflow in the Yangtze River basin, China, using a hydrological modeling approach. *Int J Digit Earth* 14(2):231–249
- Niu Z, Wang L, Feng L et al (2020) Analysis of spatiotemporal variability in temperature extremes in the Yellow and Yangtze River basins during 1961–2014 based on high-density gauge observations. *Int J Climatol* 40(1):1–21
- Ouyang R, Liu W, Fu G et al (2014) Linkages between ENSO/PDO signals and precipitation, streamflow in China during the last 100 years. *Hydrol Earth Syst Sci* 18(9):3651–3661
- Panthou G, Vischel T, Lebel T (2014) Recent trends in the regime of extreme rainfall in the Central Sahel. *Int J Climatol* 34:3998–4006
- Partridge MD, Rickman DS, Olfert MR et al (2012) Dwindling U.S. internal migration: evidence of spatial equilibrium or structural shifts in local labor markets? *Reg Sci Urban Econ* 42:375–388
- Peng J, Luo X, Liu F et al (2018) Analyzing the influences of ENSO and PDO on water discharge from the Yangtze River into the sea. *Hydrol Process* 32(8):1090–1103
- Rafiei-Sardooi E, Azareh A, Shoostari SJ (2022) Long-term assessment of land-use and climate change on water scarcity in an arid

- basin in Iran. *Ecol Model* 467:109934. <https://doi.org/10.1016/j.ecolmodel.2022.109934>
- Roxy MK, Ritika K, Terray P et al (2015) Drying of Indian subcontinent by rapid Indian Ocean warming and a weakening land-sea thermal gradient. *Nat Commun* 6:7423. <https://doi.org/10.1038/ncomms8423>
- Salzmann M, Weser H, Cherian R (2014) Robust response of Asian summer monsoon to anthropogenic aerosols in CMIP5 models. *J Geophys Res Atmos* 119:11321–11337
- Sarr MA, Zoromei M, Seidou O et al (2013) Recent trends in selected extreme precipitation indices in Senegal: A change-point approach. *J Hydrol* 505:326–334
- Shi J, Cui LL (2022) Comparison of seasonal climate in China during the cold and warm phases of ENSO. *Clim Res* 85:113–128
- Shi GX, Ye P (2021b) Assessment on temporal and spatial variation analysis of extreme temperature indices: a case study of the Yangtze River Basin. *Int J Environ Res* 18(20):10936
- Shi GX, Ye P, Yang X (2021a) Spatio-temporal variation analysis of the Biological Boundary Temperature Index based on accumulated temperature: a case study of the Yangtze River Basin. *ISPRS Int J Geo-Inf* 10(10):675
- Sohoulande Djebou DC, Singh VP (2015) Retrieving vegetation growth patterns from soil moisture, precipitation and temperature using maximum entropy. *Ecol Model* 309–310:10–21
- Tabari H (2020) Climate change impact on flood and extreme precipitation increases with water availability. *Sci Rep* 10(1):13768
- Tang SK, Qiao SB, Feng TC et al (2021) Asymmetry of probabilistic prediction skills of the midsummer surface air temperature over the middle and lower reach of the Yangtze River valley. *Clim Dynam* 57(11–12):3285–3302
- Tao H, Gemmer M, Bai YG et al (2012) Assessment of CMIP3 climate models and projected changes of precipitation and temperature in the Yangtze River Basin, China. *Clim Change* 111(3–4):737–751
- Tao YW, Wang YK, Rhoads B et al (2020) Quantifying the impacts of the three Gorges Reservoir on water temperature in the middle reach of the Yangtze River. *J Hydrol* 582:124476
- Taylor CM, Coauthors (2017) Frequency of extreme Sahelian storms tripled since 1982 in satellite observations. *Nature* 544:475–478
- Wang B., Ding QH (2006) Changes in global monsoon precipitation over the past 56 years. *Geophysical Research Letters* 33(6):L06711. <https://doi.org/10.1029/2005GL025347>.
- Wang B, Biasutti M, Byrne MP et al (2021a) Monsoons Climate Change Assessment. *B Am Meteorol Soc* 102(1):E1–E19
- Wang M, Zhang Y, Lu Y et al (2021b) Detection and attribution of reference evapotranspiration change (1951–2020) in the Upper Yangtze River Basin of China. *J. Water Clim Change* 2021
- Wei J, Wang WG, Shao QX et al (2020) Influence of mature El Niño-Southern Oscillation phase on seasonal precipitation and streamflow in the Yangtze River Basin, China. *Int J Climatol* 40(8):3885–3905
- Wu Q, Zuo Q, Han C et al (2022) Integrated assessment of variation characteristics and driving forces in precipitation and temperature under climate change: a case study of Upper Yellow River basin, China. *Atmos Res* 272:106156
- Xiao M, Zhang Q, Singh VP (2015) Influences of ENSO, NAO, IOD and PDO on seasonal precipitation regimes in the Yangtze River basin, China. *Int J Climatol* 35:3556–3567
- Yang ZP, Gao JX, Zhou CP (2011) Spatio-temporal changes of NDVI and its relation with climatic variables in the source regions of the Yangtze and Yellow rivers. *J Geogr Sci* 21(6):979–993
- Yang P, Zhang SQ, Xia J et al (2022a) Analysis of droughts and floods alternation and its driving factors in the Yangtze River basin under climate change. *Atmos Res.* <https://doi.org/10.1016/j.atmosres.2022.106087>
- Yang P, Wang WY, Zhai XY et al (2022b) Influence of terrestrial water storage on flood potential index in the Yangtze River Basin, China. *Remote Sens* 14(13):3082. <https://doi.org/10.3390/rs14133082>
- Yang P, Zhang SQ, Xia J et al (2022c) Linear and nonlinear causal relationships between the dry/wet conditions and teleconnection indices in the Yangtze River basin. *Atmos Res.* <https://doi.org/10.1016/j.atmosres.2022.106249>
- Yang P, Zhai XY, Huang HQ et al (2023) Association and driving factors of meteorological drought and agricultural drought in Ningxia, Northwest China. *Atmos Res* 289:106753. <https://doi.org/10.1016/j.atmosres.2023.106753>
- Yue Y, Yan D, Yue Q et al (2021) Future changes in precipitation and temperature over the Yangtze River Basin in China based on CMIP6 GCMs. *Atmos Res* 264:105828
- Zhang LJ, Qian YF (2003) Annual distribution features of precipitation in China and their inter-annual variations. *Acta Meteorol Sin* 17(2):146–163
- Zhang FY, Zhang ZX, Kong R et al (2019) Changes in forest net primary productivity in the Yangtze River Basin and its relationship with climate change and human activities. *Remote Sens* 11(12):1451
- Zhang SQ, Yang P, Xia J et al (2022a) Land use/Land cover prediction and analysis of the middle reaches of the Yangtze River under different scenarios. *Sci Total Environ* 833:155238
- Zhang SQ, Yang P, Xia J et al (2022b) Research and Analysis of Ecological Environment Quality in the Middle reaches of the Yangtze River Basin between 2000 and 2019. *Remote Sens* 13:4475. <https://doi.org/10.3390/rs13214475>
- Zhao YM, Xu K, Dong NP et al (2022) Projection of climate change impacts on hydropower in the source region of the Yangtze River based on CMIP6. *J Hydrol* 606:127453
- Zhou T, Gong D, Li J et al (2009) Detecting and understanding the multi-decadal variability of the east Asian summer monsoon recent progress and state of affairs. *Meteor Z* 18:455–467. <https://doi.org/10.1127/0941-2948/2009/0396>
- Zuo QT, Han CH, Ma JX (2019) Application rules and quantification methods of water resources spatial equilibrium theory. *Hydro-Sci Eng* 6:50–58

Publisher's Note Springer Nature remains neutral with regard to jurisdictional claims in published maps and institutional affiliations.

Springer Nature or its licensor (e.g. a society or other partner) holds exclusive rights to this article under a publishing agreement with the author(s) or other rightsholder(s); author self-archiving of the accepted manuscript version of this article is solely governed by the terms of such publishing agreement and applicable law.